Biomaterials Science

ROYAL SOCIETY OF CHEMISTRY

PAPER

View Article Online
View Journal | View Issue

Cite this: *Biomater. Sci.*, 2025, **13**, 6637

Soft tissue-mimicking hydrogel stiffness modulates polarisation of human monocyte-derived macrophages

Consuelo Coser, [a,b,c] Amir M. Ghaemmaghami [*b] and Jing Yang [*a,c]

Minimising the foreign body response (FBR) to implants remains an unmet clinical challenge. The mechanical properties of biomaterials, particularly stiffness, have been shown to influence macrophage activation and FBR. However, current literature on the effects of material stiffness on macrophage activation presents conflicting results. These inconsistencies may stem from the use of cell lines or murine primary cells, which do not fully represent the behaviour of primary human monocyte-derived macrophages. Additionally, many previous studies have focused on stiffness values that fall outside the physiological range of soft tissues. In this study, we investigated how variations in stiffness affect the activation status of human monocyte-derived macrophages using alginate methacrylate (ALMA) hydrogels. The hydrogel stiffness was tuned within a physiologically relevant range (0.25–4.5 kPa) to mimic the mechanical properties of soft tissues. We found that increasing hydrogel stiffness consistently upregulated pro-inflammatory markers. Specifically, the stiffest hydrogel (ALMA 6% w/v) induced higher secretion of TNF-α and increased the calprotectin-to-mannose surface maker ratio, both hallmarks of inflammatory macrophages. Moreover, macrophages cultured on stiffer hydrogels exhibited a more elongated morphology and greater spreading. These findings provide new insight into how small changes in stiffness, within a soft tissue-relevant range, can modulate the inflammatory behaviour of human macrophages. Our results, together with findings from the literature, suggest that the contradictory data on the effects of stiffness on macrophages may be attributed to other factors, such as viscoelasticity, surface chemistry, and protein absorption, which warrant further investigation.

Received 6th August 2025,
Accepted 20th September 2025

DOI: 10.1039/d5bm01187f

rsc.li/biomaterials-science

Introduction

A recurrent adverse phenomenon following biomaterial implantation is the foreign body reaction (FBR), which often leads to the formation of a fibrous capsule surrounding the implant. This response can compromise implant functionality and therapeutic efficacy.[1–4] Macrophages play a critical role in the development of FBR. Studies using immune cell knockouts in animal models have identified macrophages as the primary drivers of fibrous capsule formation.[5] Macrophages are phagocytic cells[6] that can be broadly classified as either tissue-resident or monocyte-derived. Tissue-resident macrophages are a heterogeneous population, such as Kupffer cells, Langerhans cells, and microglia, that act as sentinels within their respective tissues.[7] On the other hand, monocyte-derived macrophages differentiate locally following monocytes migration to sites of injury or infection. Although macrophages have traditionally been classified as either classically-activated (M1) or alternatively-activated (M2), it is now recognised that they exist along a continuum of activation states,[8] with M1 and M2 representing the prototypical pro- and anti-inflammatory extremes of this spectrum.[9] An important feature of macrophages is their plasticity, the ability to dynamically shift phenotypes in response to environmental cues.[10]

It is known that the mechanical properties of biomaterials, including stiffness, affect macrophage polarisation.[11,12] Several studies have reported that stiffer substrates promote M1 polarisation. For example, in a study using RAW 264.7 cells, a mouse macrophage cell line, M1 polarisation was significantly reduced on the polyethylene glycol (PEG) hydrogel with a lower modulus (130 kPa), compared to stiffer hydrogels (240 kPa and 840 kPa). Additionally, when these gels were tested *in vivo*, the softest hydrogel resulted in the thinnest layer of macrophages at the implant site.[13] Similarly, a study using polyacrylamide

[a]*Division of Regenerative Medicine and Cellular Therapies, School of Pharmacy, University of Nottingham, Nottingham NG7 2RD, UK.*
E-mail: jing.yang@nottingham.ac.uk
[b]*Immunology & Immuno-bioengineering Group, School of Life Sciences, Faculty of Medicine and Health Sciences, University of Nottingham, Nottingham NG7 2RD, UK.*
E-mail: amir.ghaemmaghami@nottingham.ac.uk
[c]*Biodiscovery Institute, University of Nottingham, Nottingham NG7 2RD, UK*

hydrogels showed that the stiff gel (323 kPa) drove THP-1-derived macrophages towards a pro-inflammatory phenotype with impaired phagocytosis, while soft (11 kPa) and medium (88 kPa) gels induced an anti-inflammatory and highly phagocytic phenotype.[14] In another work, methacrylate gelatine (GelMA) hydrogels with different stiffnesses (2, 10 and 29 kPa) were tested using primary mouse bone marrow-derived macrophages. The stiffer hydrogel induced a pro-inflammatory phenotype, increased cell spreading and promoted a more severe *in vivo* inflammatory response.[15] In contrast, the softer GelMA supported greater cell infiltration but resulted in thinner fibrotic capsule formation. Furthermore, another study examined the response of primary mouse bone marrow-derived macrophages on soft (0.3 kPa) and stiff (230 kPa) polyacrylamide hydrogels, showing that soft substrates induced less pro-inflammatory mediators than stiff ones.[16]

Conversely, other studies have reported opposite trends, highlighting the complexity of macrophage responses to substrate stiffness. One study on polyacrylamide gels, with stiffnesses ranging from 2.55 kPa to 63.53 kPa, showed that the low-stiffness gel promoted M1 polarisation in mouse bone marrow-derived macrophages, whereas the intermediate stiffness gel induced an anti-inflammatory phenotype.[17] In another study using RGD-coated soft polyvinyl alcohol gels, the softest gel (0.56 kPa) induced a stronger inflammation compared to medium (13.42 kPa) and high stiffness (56.25 kPa) gels in both RAW264.7 cells and mouse bone marrow-derived macrophages. *In vivo* experiment in C57BL/6 mice further showed that softer gels produced a thicker fibrous capsule.[18] Similarly, poly(D,L-lactide-*co*-caprolactone) scaffolds with low stiffness (<5 kPa) drove NR8383 cells, a semi-adherent rat alveolar macrophage cell line, towards M1 polarisation and chronic inflammation *in vivo*, whereas stiffer scaffolds (>40 kPa) induced M2 polarisation, tissue formation and remodelling in a rat subcutaneous model.[19] Another study examining stiffness from 6 kPa (soft) to 16 kPa (stiff) showed that increasing matrix stiffness enhanced M2 macrophage polarisation in THP-1 cells.[20] Additional evidence includes a study using fibronectin-coated polyacrylamide gels (1, 20, and 150 kPa) with murine primary bone marrow-derived macrophages and RAW264.7 cells, which found a pro-inflammatory response on the softest gel.[21] Similarly, collagen-coated polyacrylamide gels (1 and 10 kPa) in a mouse tumour model demonstrated that increased matrix stiffness led to the accumulation of M2-like macrophages.[22]

Only a limited number of studies have investigated the effects of stiffness on human primary macrophages. One study showed that increasing the stiffness of collagen/alginate hydrogels (0.1–20 kPa) promoted M2-like polarisation.[23] Similarly, another work using RGD-modified PEG-based gels found that stiffer (10.3 kPa) substrates drove macrophages towards an anti-inflammatory phenotype.[24] In a separate study, human monocyte-derived macrophages cultured on fibronectin-coated polyacrylamide gels (1 to 280 kPa) exhibited greater cell spreading and enhanced formation of actin fibres with increasing stiffness, although their phagocytic capacity was not affected. Surface markers or cytokine profiling were not quantified in their study.[25]

Despite extensive research in this field, the effect of substrate stiffness on macrophages is still unclear as findings across studies have often been contradictory. Additionally, most studies have predominantly relied on cell lines or murine primary cells, with limited investigation using primary human monocyte-derived macrophages. These models have significant limitations due to both interspecies differences[26–29] and the differences between primary cells and cell lines,[30,31] potentially compromising the translatability of findings to human biology. Another limitation is the use of stiffness ranges that do not reflect the mechanical properties of native soft tissues, which are usually the intended targets in regenerative medicine applications involving hydrogels. Tissues such as the brain, fat, pancreas, kidneys, and liver typically exhibit a Young's modulus below 10 kPa.[32] For example, the stiffness of different pancreatic regions ranges between 1.15 ± 0.17 kPa and 2.09 ± 0.33.[33,34] In pathological conditions, such as pancreatic ductal adenocarcinoma[35] and chronic pancreatitis,[36] the stiffness increases to approximately 2.89–4.3 kPa, reaching values as high as 5.8 kPa in long-term chronic pancreatitis.

To have a better understanding on how stiffness affects macrophage polarisation, we investigated the activation status of human monocyte-derived macrophages on methacrylate alginate (ALMA) hydrogels with mechanical properties mimicking soft tissues. Alginate-based hydrogels due to their low cost, low toxicity, abundance, and ease of chemical modification[37–40] have been explored in the context of immunomodulatory biomaterials.[41] Mechanical tuneability and chemical versatility make ALMA a valuable material for investigating macrophage responses in the context of FBR. However, despite extensive research, an alginate-based material that fully prevent FBR have yet to be achieved, representing a key barrier to a successful clinical translation.

The mechanical properties of the hydrogels were determined using rheological testing. Monocytes were isolated from healthy blood donors and cultured on ALMA hydrogels for 6 days. Macrophage phenotype was assessed using a combination of techniques, including morphological evaluation, surface marker expression and cytokine profiling. We observed that increasing hydrogel stiffness promoted a pro-inflammatory macrophage phenotype, as evidenced by elevated TNF-α secretion, an increased calprotectin-to-mannose receptor ratio, and a more elongated cell morphology.

Materials and methods

Materials

Alginate methacrylate (degree of metahcrylation: 20%–40%), 2-hydroxy-4′-(2-hydroxyethoxy)-2-methylpropiophenone (Irgacure D-2959), 3-(trimethoxysilyl)propyl methacrylate, toluene, PBS, Tween20, RPMI-1640, fetal bovine serum (FBS), penicillin–streptomycin, L-glutamine, glycine, trypan blue solution, Macrophage Colony-Stimulating Factor (M-CSF), Granulocyte-Macrophage

Colony-Stimulating Factor (GM-CSF), Interferon-γ (IFN-γ), human recombinant IL-4, and goat serum were purchased from Sigma Aldrich. Sulfuric acid 1 N, anti-human calprotectin mouse immunoglobulin G1, TMB substrate kit, and LIVE/DEAD viability kit, Pierce™ chromogenic endotoxin quant kit were supplied by Thermo Scientific, UK. ToxiLight™ non-destructive cytotoxicity BioAssay kit and 100% lysis control set were purchased from Lonza. Buffy coats were obtained from healthy donors (National Blood Service, Sheffield, UK) after obtaining informed written consent and following ethics committee approval (Research Ethics Committee, Faculty of Medicine and Health Sciences, University of Nottingham). Ficoll-Plaque PREMIUM sterile solution was purchased by cytiva. LS columns, pre-separation filters (30 mm), and CD14 MicroBeads UltraPure human were bought from Miltenyi Biotec. Anti-human CD206 (MR) rabbit IgG1 primary antibody was provided by Abcam. Phalloidin-iFluor 594 was supplied by AAT Bioquest, Stratech. 4,6-Diamidino-2-phenylindole (DAPI), UltraPure EDTA (0.5 M, pH 8), AlexaFluor 488 goat anti-mouse IgG (H + L), and Texas Red-X goat anti-rabbit IgG (H + L) were purchased from Invitrogen. DuoSet® ELISA kits (TNF-α, IL-6, IL-10, CCL18) were purchased from Biotechne®|R&D systems.

Coverslips silanisation

Coverslips were functionalised as previously described with some modifications.[42] Plasma cleaning (O_2 100%, 10 min) was performed on glass coverslips (d = 16 mm), which were subsequently silanised with 3-(trimethoxysilyl)propyl methacrylate (2% v/v) in dry toluene for 24 h. The reaction was carried out under argon atmosphere. Coverslips were washed with fresh toluene (×2), acetone (×3), and dried under vacuum for 7 days prior to use.

Preparation of ALMA hydrogels

To fabricate ALMA hydrogel, Irgacure D-2959 aqueous solution (0.5% w/v) was prepared and subsequently added to alginate methacrylate powder. ALMA solutions (2%, 4%, and 6% w/v) were stirred overnight and underwent photo-crosslinking with UV light (365 nm) for 10 minutes. Samples that were used for the rheological characterisation were prepared as discs (2 mm, r = 1.06 cm^2). Samples that were used for cell culture were prepared as thin film on silanised coverslips by creating a "sandwich" system with glass slides. UV-sterilization (260 nm) was performed for 40 minutes and samples were then left in penicillin–streptomycin (10×) overnight. Samples were washed 5 times with sterile PBS and incubated with RPMI-1640 (FBS 10% v/v, penicillin–streptomycin 1% v/v, L-glutamine 1% v/v) for 24 hours prior cell seeding.

In vitro hydrogel swelling

Hydrogels were immersed in 15 mL PBS at 37 °C and weighed multiple times over a 6-day period. The swollen weight was expressed as a percentage increase from the initial hydrogel weight, recorded immediately after UV photo-crosslinking.

Environmental scanning electron microscopy (ESEM)

Hydrogels were prepared and left equilibrating in PBS for at least 24 h prior the analysis. Samples were placed in a FEI Quanta 650 ESEM and images were captured using an optimised working distance for each sample at 5–10 kV, while humidity was kept between 88.9–96.3%.

Optical profilometry

Surface roughness of hydrated ALMA hydrogels was measured using an optical profilometer. Gels were equilibrated in PBS, blotted to remove excess liquid, and mounted on the stage. Scans were acquired with a 50× objective over a 340 × 261 μm^2 area, with 3 regions per sample to account for heterogeneity. Arithmetical mean height (S_a) and root mean square height (S_q) were extracted from topography maps using the instrument's analysis software (Zeta 3D Analysis).

Mechanical characterisation

Rheological measurements were performed with Anton-Paar rheometer, equipped with a 25 N load cell. Discs of ALMA hydrogels were prepared ahead the measurements and incubated in PBS until they reach the equilibrium swelling. Amplitude sweeps was carried out at a constant frequency of 1 Hz, between 1% and 1000% of shear strain. Frequency sweep was conducted within the linear viscoelastic (LVE) range, at a constant shear strain of 5%; storage and loss moduli were extrapolated at frequency 1 Hz. Stress relaxation was performed within the LVE range, at a constant shear strain of 5%; relaxation modulus was recorded for 200 s and expressed as a percentage decrease from the initial relaxation modulus.

Mesh size measurement

Rubber elasticity theory was used to calculate mesh size of ALMA hydrogels. The crosslinking density ρ_x (mol m^{-3}) is determined from the storage modulus (G', Pa), the universal gas constant (R, J mol^{-1} K^{-1}), and the absolute temperature (T, K), as shown in

$$\rho_x = \frac{G'}{RT}. \quad (1)$$

The mesh size ξ (m) is then calculated from the crosslinking density (ρ_x) and Avogadro's number N_A, according to eqn (2).[43]

$$\xi = \sqrt[3]{\frac{6}{\pi \rho_x N_A}} \quad (2)$$

X-Ray photoelectron spectroscopy

All samples were mounted onto stainless steel stubs using carbon sticky tabs. X-ray Photoelectron Spectroscopy (XPS) was conducted using a Kratos Axis Ultra DLD with a monochromatic Al X-ray source (1486.6 eV, 15 kV, 10 mA). Wide and high-resolution scans were conducted in addition to the measurement C 1s for calibration: charge corrected to 284.8 eV. Parameters for wide scan acquisition were as follows: 160

eV of pass energy, step size of 0.5 eV, and 1200 s of scan time. Parameters for high resolution scan acquisition were as follows: 20 eV of pass energy, step size of 0.1 eV, and 1200 s of scan time. Binding energies were measured over a range of 0–1300 eV. All spectra were analysed in CasaXPS constraining the Full Width at Half Maximum (FWHM) to the same value for all deconvoluted spectral peaks for the same element.

Monocyte isolation and differentiation

Buffy coats from healthy donors were obtained from the National Blood Service (Sheffield, UK). All experiments were conducted in compliance with the Declaration of Helsinki and the Human Tissue Act (2004), following ethics committee approval (2009/D055 Research Ethics Committee, Faculty of Medicine and Health Sciences, University of Nottingham). Informed consent was obtained from all donors prior to sample collection. Monocytes were isolated through positive selection (CD14 magnetic beads), using MACS magnetic cell separation system. Isolated monocytes were prepared to a cell density of 1×10^6 cell per mL in RPMI-1640 medium (10% FBS, 1% L-glutamine, 1% streptomycin and penicillin, 10 ng mL^{-1} M-CSF) and seeded on ALMA hydrogel. To ensure cells were only seeded on the hydrogels, non-cultured-treated plates were used, and media was changed after 24 h to remove floating monocytes. Cells were incubated in a humidified incubator maintained at 37 °C and 5% CO_2 for 6 days (37 °C, 5% CO_2) until differentiation was completed; fresh media was added on day 3. Media was supplemented with M-CSF (10 ng mL^{-1}) on day 1 and 3 to induce the differentiation into naïve macrophages. As a reference, monocytes were also cultured on tissue culture plastic at the same cell density and conditions.[44]

Live/dead viability assay

On day 6, media was removed, and macrophages were incubated with PBS containing a mixture of green-fluorescent calcein-AM (1 : 2000) and red-fluorescent ethidium homodimer-1 (1 : 500) for 30 minutes at 37 °C and 5% CO_2. Cells were imaged using an Olympus IX51 fluorescence microscope, with 10× objective.

Cytotoxicity measurement by using the ToxiLight assay

20 μL of culture supernatant was collected and added to a white assay plate. 100 μL of adenylate kinase detection reagent was added and incubated at room temperature (RT) for 5 minutes. Luminescence was read using a plate reader (Promega GloMax® explorer). A negative (M0 macrophages cultured on TCP) and positive (M0 macrophages cultured on TCP and lysed after 6 days of culture using the Toxilight™ 100% lysis reagent) were included.

Endotoxin quantification assay

ALMA 6% hydrogels were incubated with PBS (1.5 mL) in humidified incubator maintained at 37 °C and 5% CO_2 for 6 days (37 °C, 5% CO_2) to simulate cell culture conditions. Endotoxin standard solutions (0.1–0.01 EU per mL) and samples (50 μL) were added to 96-well plate and incubated with amoebocyte lysate solution (50 μL) for 25 minutes at 37 °C. Chromogenic substrate solution (100 mL) was added and incubated for 6 minutes at 37 °C. Acetic acid 25% v/v (50 μL) was added as stop solution and absorbance was read at 405 nm using a plate reader (Promega GloMax® explorer). The endotoxin concentration in each condition was calculated using a 4-point standard curve.

Immunostaining of macrophages

Macrophages were fixed by incubation in paraformaldehyde 4% v/v (in PBS) for 15 min on day 1, day 3, and day 6. On day 1 and 3, cells were washed 3 times with 0.2% Tween-20 in PBS (0.2% v/v) followed by a blocking step with BSA (3% w/v) and glycine (1%) in PBS. Cells were washed 3 times with 0.2% Tween-20 in PBS and incubated with Phalloidin-iFluor 647 (1 : 1000) and DAPI (1 : 5000) in PBS (BSA 1% w/v) for 1 hour at RT. On day 6, cells were washed 3 times with 0.2% Tween-20 in PBS and two blocking steps were subsequently performed, firstly with BSA (3% w/v) and glycine (1%) in PBS, then with goat serum (5%) in PBS. Macrophages were washed 3 times with 0.2% Tween-20 in PBS and incubated with anti-human calprotectin mouse immunoglobulin G1 (IgG1) antibody (2 mg mL^{-1}) and anti-human CD206 (MR) rabbit IgG1 primary antibody (1 mg mL^{-1}) overnight at 4 °C. Cells were washed 3 times with 0.2% Tween-20 in PBS and incubated with AlexaFluor-488 goat anti-mouse IgG (8 mg mL^{-1}) and Rhodamine Red goat anti-rabbit IgG secondary antibody (8 mg mL^{-1}) for 1 hour at RT. Cells were further incubated with Phalloidin-iFluor 594 (1 : 1000) and DAPI (1 : 5000) in PBS (BSA 1% w/v) for 1 hour at RT. Cells were washed 3 times with PBS and imaged using a Leica TCS SPE confocal microscope.[45] Image analysis was performed using CellProfiler software (https://www.cellprofiler.org/) to quantify the cell number, the eccentricity, the cell area, and the fluorescent signal corresponding to calprotectin and mannose receptor markers.

Enzyme-linked immunosorbent assay (ELISA)

For TNF-α, IL-6, IL-10, and CCL18, 384-plates were coated with 25 μl capture antibody (TNF-α: 4 μg mL^{-1}, IL-6, IL-10, and CCL18: 2 μg mL^{-1}) overnight on a rocker at RT. ELISA plates were washed 3 times with PBS containing 0.05% tween-20 (100 μl) and blocked with 75 μL BSA 1% w/v for 1 hour at RT. Supernatant was thawed and brought to RT. Plates were washed 3 times with PBS containing 0.05% tween-20 (100 μL) and incubated with 25 μL supernatant and standard solutions (TNF-α: 1000–15.6 pg mL^{-1}, IL-6: 600–9.38 pg mL^{-1}, IL-10: 2000–31.2 pg mL^{-1}, and CCL18: 500–7.81 pg mL^{-1}) for 2 hours on a rocker at RT. Plates were washed 3 times with PBS containing 0.05% tween-20 (100 μL) and incubated with 25 μL detection antibody (TNF-α, IL-6, and IL-10: 50 ng mL^{-1}, CCL18: 100 ng mL^{-1}) for 2 hours on a rocker at RT. Plates were washed 3 times with PBS containing 0.05% tween-20 (100 μl) and incubated with 25 μL streptavidin-HRP conjugate (40-fold diluted) for 20 minutes while protected from light on a rocker at RT. Plates were washed 3 times with PBS containing 0.05% tween-20 (100 μL) and incubated with 25 μL TMB substrate for

20 minutes while protected from light on a rocker at RT. Sulfuric acid 1 N (12.5 μL) was added as stop solution and absorbance was read at 450 nm and 570 nm using a plate reader (Promega GloMax® explorer). The cytokine concentration in each condition was calculated using a 7-point standard curve.

Statistical analysis

Hydrogel characterisation data is presented as mean ± standard deviation (SD) with each experimental condition tested in triplicate. Mechanical property and endotoxin data is presented as mean ± standard deviation of three experimental repeats (n = 3) per condition. Cell culture data is presented as mean ± standard error of mean (SEM) from three independent experiments (N = 3), each with three experimental repeats (n = 3) per condition. Statistical analysis was carried out in GraphPad PRISM 9.0. One-way ANOVA was performed to determine significant differences between experimental conditions (α = 0.05). Tukey's *post hoc* test was performed for pair-wise comparisons. Pairs with significant differences were labelled as $*p \leq 0.05$, $**p < 0.01$, $***p < 0.001$ and $****p < 0.0001$.

Results & discussion

In vitro swelling (Fig. 1B) showed that all three hydrogel compositions reached equilibrium in less than 24 hours, with ALMA 4% and 6% exhibiting a similar weight increase of 20%. The composition with 2% methacrylate alginate showed a higher swelling, reflecting the lower concentration of the polymer involved in forming the 3D network. To quantitatively determine the mesh size, amplitude sweeps (Fig. S1) were performed, and the rubber elasticity theory was applied to relate the storage modulus (G') to the network crosslinking density.[43,46,47] Increasing ALMA concentration led to significantly smaller mesh sizes, showing an inverse correlation with stiffness (Fig. 1C). This observation is consistent with the fact that higher polymer concentrations yield stiffer hydrogels by forming denser crosslinked networks, which reduces both void space and the swelling capacity.[48] Environmental scanning electron microscopy (ESEM) images (Fig. 1D) were collected to characterise the surface of hydrogels at different ALMA concentrations in their native hydrated state. To complement ESEM observations, we further characterised surface topography using optical profilometry. Profilometry of hydrated gels provided quantitative roughness parameters, including the arithmetical mean height (S_a) and root mean square height (S_q). Roughness was higher for ALMA 2% (S_a = 41.6 nm; S_q = 53.4 nm) compared with ALMA 4% (S_a = 26.2 nm; S_q = 33.4 nm) and 6% (S_a = 24.3 nm; S_q = 30.7 nm), while no significant differences were observed between the 4% and 6% hydrogels (Fig. S2A and S2B). Both ESEM and profilometry indicated that surface smoothness increased with polymer concentration.

Protein adsorption and surface chemistry were assessed by XPS (Fig. 1E). Analysis of the integrated N 1s peaks, which arise exclusively from adsorbed proteins as ALMA lacks nitrogen, showed no significant differences in nitrogen content among the compositions (Fig. 1F), indicating comparable protein adsorption across all formulations. Similarly, the quantification of C 1s (Fig. 1G) and O 1s (Fig. 1H) peaks revealed no detectable changes in surface functional groups with increasing polymer concentration. It is important to note that XPS provides only elemental composition and relative abundance of elements and cannot determine the identity, conformation, or orientation of the adsorbed proteins. Complementary approaches, such as mass spectrometry, would be required to fully characterise the adsorbed protein layer.

The mechanical properties of ALMA hydrogels were determined using rheological assessments after reaching equilibrium swelling. Frequency sweeps (Fig. 2A) were carried out within the LVE, previously determined through amplitude sweeps, to quantify the storage (G') and loss (G'') moduli (Fig. 2B), and the complex viscosities (Fig. 2C) of the ALMA hydrogels. While ALMA 2% and 4% did not show a significant difference in their G' (257.9 Pa and 1195.7 Pa, respectively) and G'' values (33.8 Pa and 35.2 Pa, respectively), the ALMA 6% hydrogel exhibited significantly higher moduli (G' value of 4426.6 Pa and G'' value of 175.3 Pa) compared to the two softer hydrogels. Together, these three compositions span stiffness values across the physiologically relevant range of soft tissues – from very soft tissues, such as the lens (0.2–0.8 kPa), to intermediate tissues, including the thyroid (1.3 kPa), pancreas (1.1 kPa), lung (1.5 kPa), adipose tissue (1.6 kPa), liver (2 kPa), and brain (1 kPa), and to relatively stiffer organs such as the kidney (4–5 kPa)[32] – thus enabling investigation of cell responses across a representative mechanical spectrum. Stress relaxation was also investigated as many studies have shown the effect of viscoelasticity on cell responses.[49–51] All three hydrogels showed similar stress relaxation profiles (Fig. 2D), confirming that observed differences in macrophage activation status were due to stiffness rather than viscoelasticity.

To provide an overview of the experimental strategy used to investigate macrophage responses to hydrogel stiffness, a schematic representation is shown in Fig. 3.

A live/dead assay (Fig. 4A) was performed to assess the toxicity of ALMA hydrogels. The data showed that macrophages remained viable after 6 days of culture across all hydrogels, suggesting comparable biocompatibility. The high cell viability was also supported by the ToxiLight assay which showed no significant differences in metabolic activity between macrophages cultured on the hydrogels and those cultured on TCP controls (Fig. 4B). Together, these results demonstrated the suitability of ALMA hydrogels as biocompatible substrates for macrophage differentiation and culture.

The expression levels of calprotectin (pro-inflammation marker) and mannose receptor (anti-inflammatory markers) were quantified by immunofluorescent staining and image analysis, in line with our previous works[52] (Fig. 5A). To ensure cross-sample comparisons, the number of imaged cells was quantified across the different hydrogels. No significant differ-

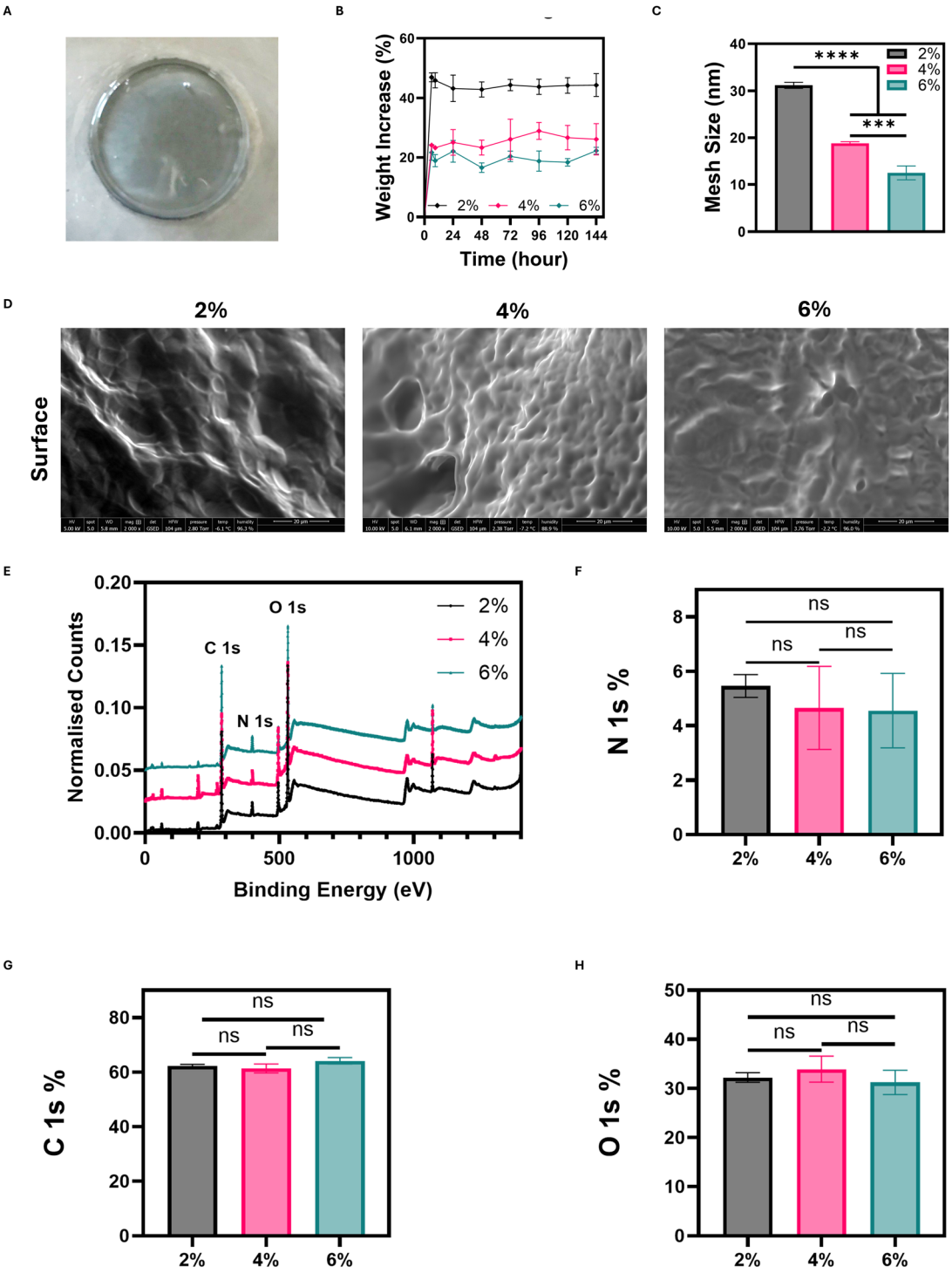

Fig. 1 Swelling, mesh size, surface morphology and surface adsorbed proteins. (A) Gross view of an ALMA hydrogel disc. (B) Swelling equilibrium and (C) mesh size of ALMA hydrogels at 2%, 4%, and 6% w/v calculated by using the rheological data and the rubber elasticity theory. (D) Representative environmental scanning electron microscopy (ESEM) images of the hydrogel surfaces. (E) XPS wide-scan spectra of ALMA hydrogels following 24-hour incubation in serum-containing culture medium. Quantification of (F) N 1s, (G) C 1s, and (H) O 1s peaks.

ences in cell number were detected (Fig. 5B). The calprotectin-to-mannose expression ratio was used as a surrogate for assessing the macrophage activation status (Fig. 5C). There was no significant difference in the calprotectin-to-MR ratio between macrophages cultured on ALMA 2% and 4%. Macrophages cultured on 2% and 4% ALMA expressed more MR relative to calprotectin as the ratios were below one. In contrast, calprotectin was expressed significantly more (*ca.* 6-fold) in macrophages

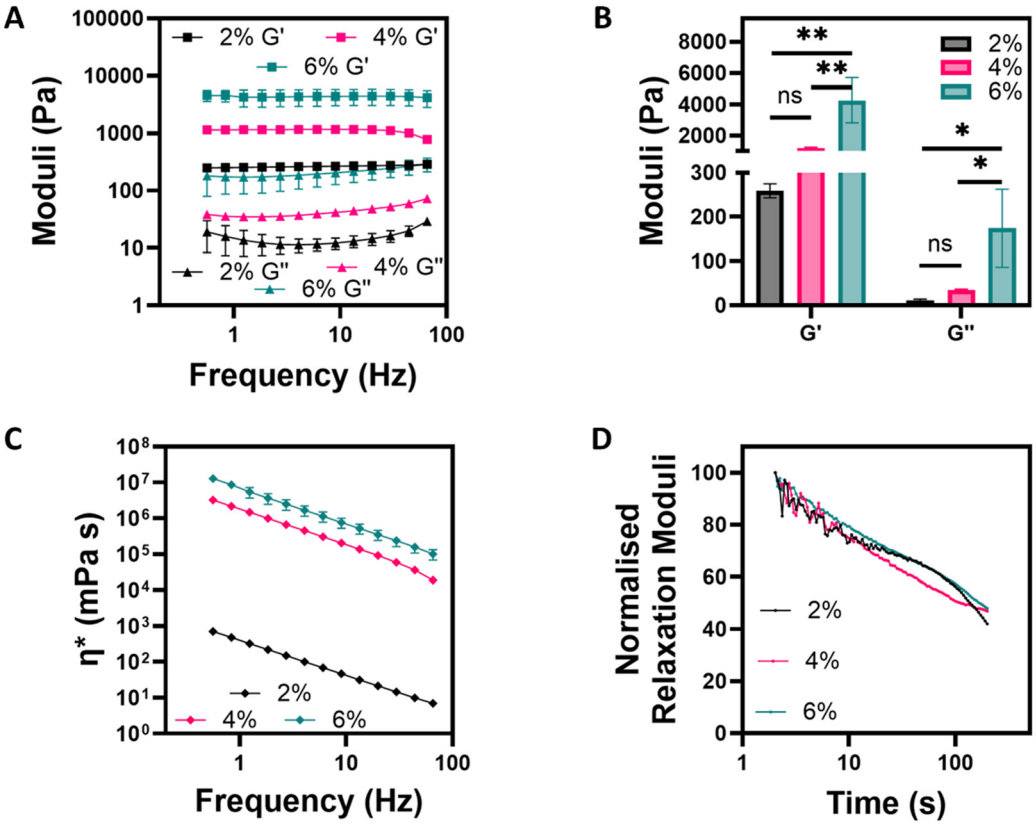

Fig. 2 Rheological characterisation of methacrylate alginate. (A) Frequency sweeps, (B) storage (G') and loss (G'') moduli, (C) complex viscosity, and (D) normalised stress relaxation of ALMA hydrogels. Frequency sweeps and stress relaxation were performed within LVE region (5% strain).

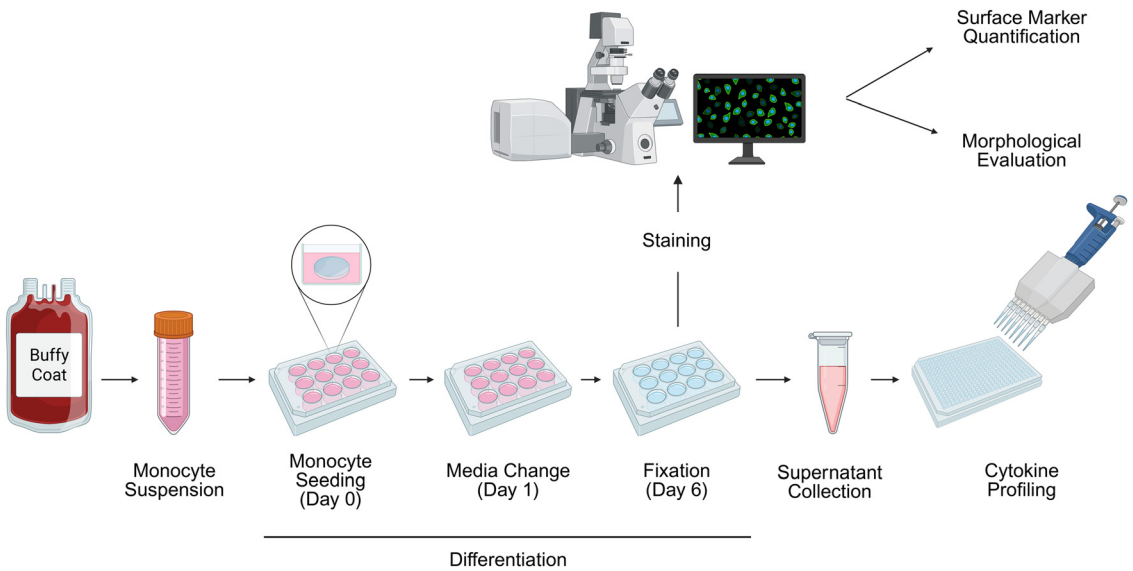

Fig. 3 Overview of the experimental workflow. Monocyte isolation from healthy blood donor, differentiation and characterisation of morphology, surface markers and cytokine profiling of macrophages.

that were cultured on ALMA 6%. This suggested that a significant increase in the storage modulus (G') promoted a shift towards a more pro-inflammatory, M1-like phenotype.

To further characterise macrophage activation in response to different stiffnesses, monocytes were stained for nuclei and F-actin to monitor their morphology over the 6-day culture

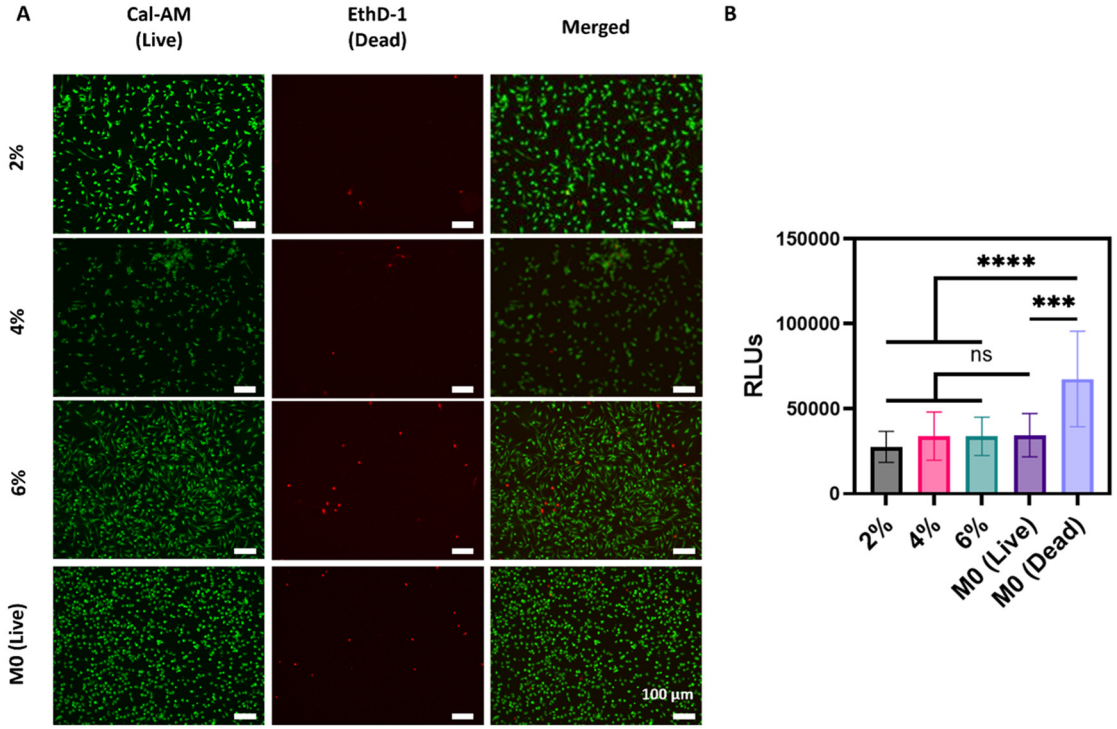

Fig. 4 Human primary macrophage viability on methacrylate alginate. (A) Fluorescent microscopy images of macrophages stained for calcein-AM (green – live cells) and ethidium homodimer-1 (red – dead cells) at day 6. Scale bar: 100 µm. (B) ToxiLight assay on macrophages cultured for 6 days on ALMA 2%, 4%, and 6%. Positive control (M0 (dead)) is purposely lysed macrophages. M0 macrophages cultured on tissue culture plastic (M0 (live)) were used as negative controls.

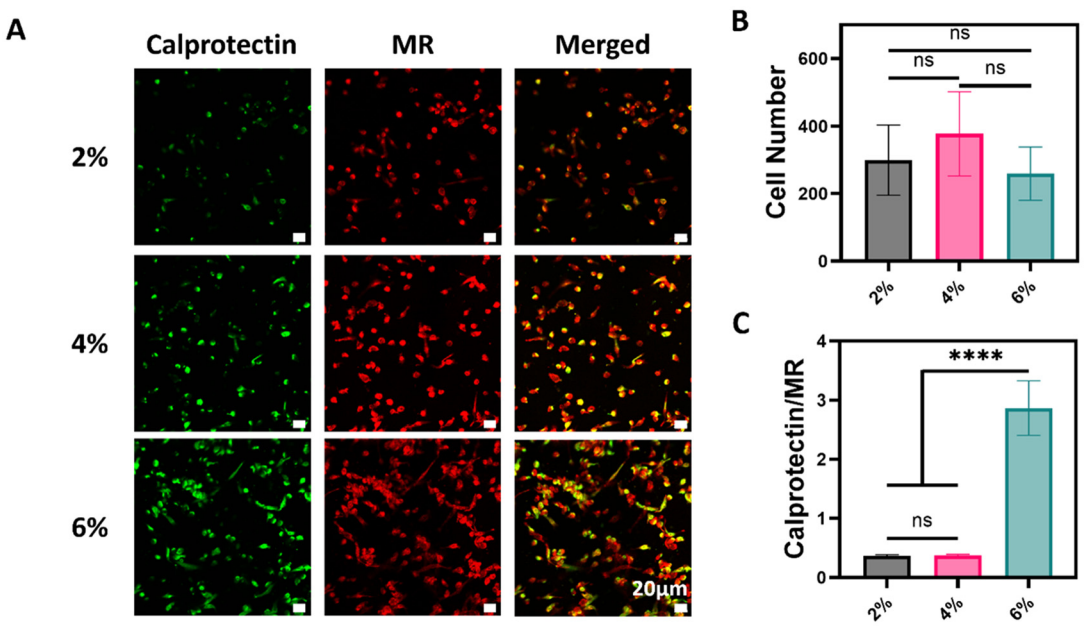

Fig. 5 Human macrophage polarisation characterised by surface markers on different ALMA hydrogels. (A) Confocal microscopy images of macrophages stained for pro- (calprotectin – green) and anti- (mannose receptor – red) inflammatory surface markers at day 6. Scale bar: 20 µm. (B) Quantification of cell numbers cultured on ALMA hydrogels at day 6. (C) Ratio between calprotectin and MR fluorescent signals.

period. As shown in Fig. 6A and B, cells cultured on ALMA 6% presented a more elongated morphology starting from day 3, in contrast to those on the softer hydrogels, which maintained a rounder shape. To quantitatively compare cell morphologies, parameters including cell eccentricity and area were measured. Eccentricity was used to quantify cell elongation, where a value

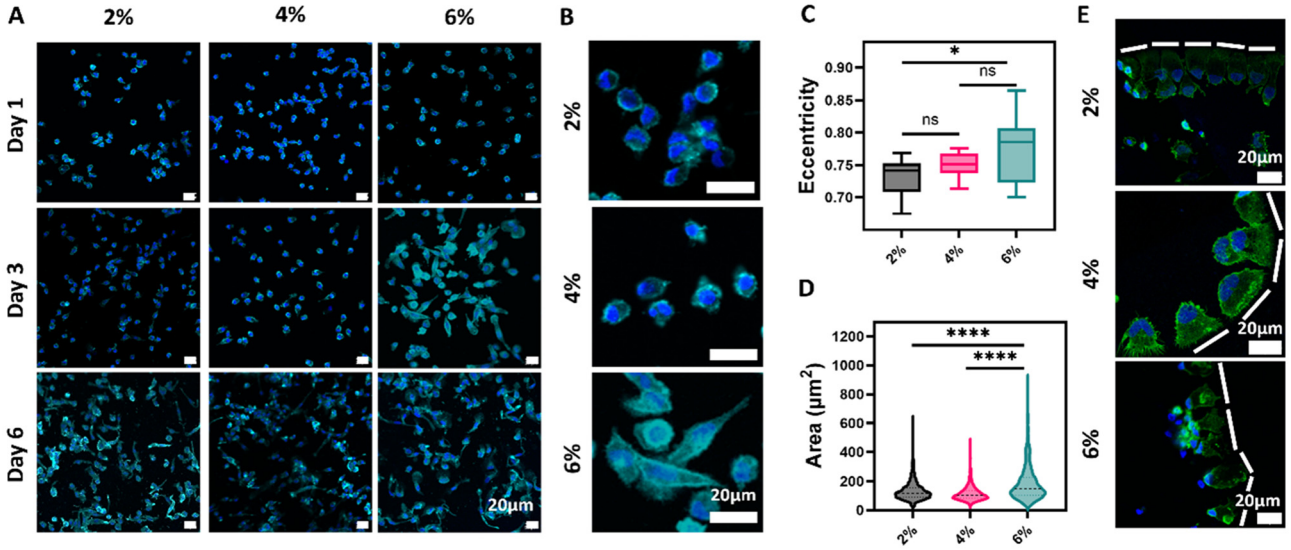

Fig. 6 Human macrophage morphology on different alginates. (A) Confocal microscopy images of monocyte (day 1 and 3) and macrophages (day 6) stained for nuclei (DAPI – blue) and F-actin (Phalloidin – cyan) at day 1, day 3, and day 6. Scale bar: 20 μm. (B) Zoomed-in confocal microscopy images representative of macrophage morphology at day 3. Scale bar: 20 μm. (C) Quantification of eccentricity and (D) area of macrophages at day 6. (E) Representative morphologies of macrophages adhered close to the edge of the disk-shaped ALMA hydrogels. White dashed lines represent the edges. Scale bar: 20 μm.

of zero corresponds to a perfect circle and one to a line. On day 6, macrophages on the stiffest ALMA hydrogel (ALMA 6%) displayed significantly higher eccentricity (~0.8) compared to those on the softest hydrogel (ALMA 2%), which showed eccentricity values below 0.75 (Fig. 6C). Similarly, the cell area was significantly larger on the stiffest hydrogel (~197 μm^2) than on the softest substrate (~120 μm^2), suggesting decreased cell interaction with the softer materials (Fig. 6D).

Interestingly, cells located near the edge of the disk-shaped hydrogels consistently exhibited much greater spreading compared to those resided on more central regions (Fig. 6E). This phenomenon was observed for all the three ALMA concentrations. The spreading appeared to be unidirectional towards the edge, evidenced by the cell lamellipodia distribution. This unexpected edge-related cell morphology might be due to a higher local stiffness near the perimeter, potentially caused by increased water evaporation near the edge during hydrogel preparation. However, the local stiffness and composition will need further characterisation in future studies to elucidate the underlying mechanisms.

To further determine the phenotype of macrophages on different ALMA hydrogels, pro- (TNF-α, IL-6) and anti- (IL-10, CCL18) inflammatory cytokines were quantified by using sandwich ELISA (Fig. 7). TNF-α secreted from macrophages cultured on ALMA 6% was significantly higher compared to cells on ALMA 2% and 4%, suggesting a shift towards a pro-inflammatory phenotype on the stiffer substrate. Although no significant difference was observed for IL-6, a trend of increasing secretion with increasing stiffness was observed. In terms of anti-inflammatory cytokines, IL-10 secretion was significantly higher from macrophages cultured on the softest ALMA 2%. Although no significant difference was observed for CCL18 release, a decreasing trend with increasing stiffness was observed. Overall, the cytokine profile supported the observation that stiffer hydrogels induced a pro-inflammatory phenotype, whereas softer substrates showed an anti-inflammatory activation status.

It is known that high endotoxin levels can induce pro-inflammatory polarisation in macrophages.[53] To exclude the possibility that changes in cell behaviour were a consequence of high endotoxin levels, ALMA 6% was prepared and incubated in PBS, simulating the cell culture conditions. After 6 days, endotoxins were quantified and data showed that their level was below the accepted limit of 0.1 EU per mL for *in vitro* immunogenicity assays, which excluded the possibility of the influence of endotoxins on macrophage activation status (Fig. S3).

Discussion

The conflicting reports on macrophage responses to substrate stiffness, along with the relatively high stiffness ranges commonly investigated in the literature, prompted us to study human macrophages on soft hydrogels. We prepared hydrogels with different mechanical properties by varying ALMA concentrations from 2% to 6% w/v. Our results showed that even a modest increase (in absolute value) from ~0.25 kPa to ~4.5 kPa led to significant changes in human monocyte-derived macrophages. Our results demonstrated that cells cultured on the stiffest substrate (ALMA 6%, ~4.5 kPa) showed a more elongated morphology as early as day 3. This feature was also

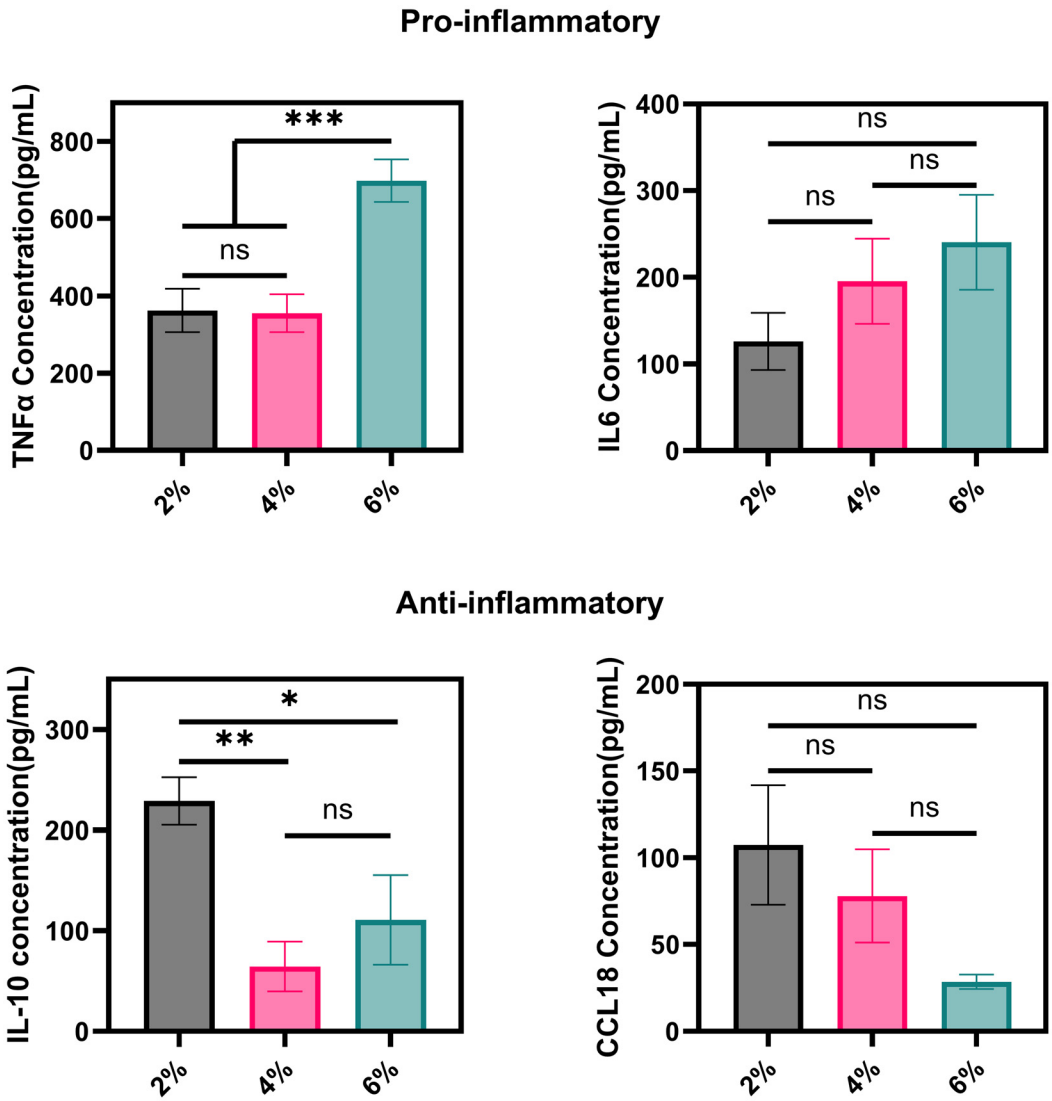

Fig. 7 Quantification of pro- (TNF-α, IL-6) and anti- (IL-10, CCL18) inflammatory cytokines secreted by macrophages at day 6.

associated with a higher calprotectin-to-mannose receptor expression ratio, and a significant increase in pro-inflammatory cytokine release, particularly TNF-α. A stiffness-dependent increase in IL-6 was also observed when moving from soft (ALMA 2%) to stiff (ALMA 6%) hydrogels.

The stiffness-dependent trend observed in our study aligns with several previous reports in which increased stiffness promoted a shift towards M1-like macrophage phenotype. Blakney *et al.* reported increased TNF-α, IL-1β, and IL-6 expression in macrophages cultured on stiff PEG gels (840 kPa),[13] while Sridharan *et al.* found greater cell spreading and upregulation of two pro-inflammatory chemokines, such as CXCL11 and CCL20, on stiff polyacrylamide gels (323 kPa).[14] In both studies, softer gels (>11 kPa) promoted an anti-inflammatory phenotype. Similarly, Zhuang *et al.* showed that increasing GelMA stiffness (2–29 kPa) enhanced inflammatory signalling and M1 polarisation.[15] Our findings are also consistent with those of Previtera *et al.*, who showed reduced pro-inflammatory mediator release on soft gels (0.3 kPa) compared to stiff ones (230 kPa).[16] Although these reported findings align with our data, it is important to note that most of the previously defined "soft" substrates are still 2–3 orders of magnitude stiffer than our ALMA 2% hydrogel (~0.25 kPa), with the exception of the soft gel used by Previtera *et al.* These reported soft hydrogels are even at least 2-fold stiffer than our stiffest gel (ALMA 6%, ~4.5 kPa). Notably, our findings extend and expand the existing knowledge by demonstrating that stiffness-driven M1 activation is not limited to high-stiffness substrates (>10 kPa) but can also arise within the low-kilopascal range. This is particularly relevant in the context of soft tissues, both in healthy and fibrotic conditions. For example, in the liver and brain, stiffness can increase from 0.3–1 kPa under healthy conditions to >25 kPa during fibrosis.[54,55] These results highlight the need for comparative studies which focus on the low-

kPa range to elucidate how subtle changes in the mechanical properties of soft tissues influence macrophage behaviour.

Several studied reported an opposite trend to what we and others observed, showing a pro-inflammatory phenotype associated with softer gels.[18–22] Such discrepancies might depend on other factors than stiffness alone. In fact, stiffness is not the only mechanical property of hydrogels. Viscoelasticity is another key feature[56] and changing the degree of crosslinking in a 3D polymer network can alter the viscoelastic properties of hydrogels.[57–59] Viscoelasticity has been shown to modulate mechano-sensitive molecular pathways in various cell types,[51] such as fibroblasts and cancer cells,[59] hepatocytes,[60] and human induced pluripotent stem cells.[61] Kalashnikov N. *et al.* have directly addressed how viscoelastic cues modulate THP-1 macrophage morphology and functions, revealing that more viscous substrates induce a rounder morphology and a reduced phagocytic activity.[49] Despite this, studies examining the role of viscoelasticity in macrophage behaviour remain scarce. Further research is needed to elucidate how viscoelastic properties affect macrophages, particularly in the context of FBR.

Another factor that may explain the divergent results is the source of macrophages used in different studies.[62] It is worth noting that most studies used murine bone marrow-derived macrophages, RAW264.7 cells[18] or NR8383 rat alveolar macrophages,[19] all of which may exhibit different sensitivities and responses to mechanical cues compared to human macrophages. Only a few studies have used primary monocyte-derived macrophages, and interestingly they showed trends opposite to ours. Guenther *et al.* showed that increased stiffness led to a M2-like phenotype, with macrophages on stiffer substrates expressing higher levels of CD206 and MMP13.[23] However, their study involved coculture with cancer cells, introducing additional variables such as tumour-macrophage crosstalk that can independently affect macrophage phenotype. Furthermore, the use of a 3D culture system in their study adds complexity, as dimensionality is also known to impact macrophage behaviour.[63] Similarly, Scott *et al.* reported that human macrophages cultured on stiffer RGD-modified-PEG-based gels (10.3 kPa) displayed a shift towards an anti-inflammatory phenotype.[24] Adlerz *et al.* also studied human monocyte-derived macrophages on fibronectin-coated polyacrylamide gels of varying stiffness.[25] While their findings addressed morphological changes, they did not include key phenotypic indicators such as surface marker expression or cytokine secretion, making it difficult to determine whether substrate stiffness promoted a pro- or anti-inflammatory state.

Surface chemistry plays a critical role in modulating cell-biomaterial interactions, primarily by influencing the adsorption of proteins from serum or culture media onto the substrate surface.[64] The amount, composition, and conformation of the adsorbed protein layer vary depending on the material's chemical properties, and this layer critically determines the presentation of adhesive motifs to cells. Hydrogels can also be functionalized with peptides, such as RGD-containing sequences,[24] or extracellular matrix proteins, such as fibronectin or collagen,[21,25] that favour cell attachment, promoting a stronger integrin engagement compared to unmodified hydrogels, which rely solely on non-specifically adsorbed proteins. These variations directly affect how integrins engage with the substrate, as integrin-based adhesion complexes serve as key mechano-transduction bridges between the extracellular environment and the cytoskeleton.[65] As a result, variations in protein adsorption and differences in surface densities of binding motifs can influence cell adhesion and mechano-transduction pathways, independently from the mechanical properties of the gels. Ultimately, these changes can affect gene expression and functional responses in cells, including macrophages, as demonstrated in previous studies.[66–69] This may partly explain the divergent polarisation outcomes observed across different studies using hydrogels with comparable stiffness but different surface chemistries.

Other features, such as surface roughness and mesh size, can influence macrophage responses, as previously reported in the literature.[70,71] However, our data indicate that their contribution is minimal in our system, with stiffness emerging as the dominant factor shaping cellular behaviour. For example, although ALMA 4% and 6% exhibited comparable roughness but different stiffnesses, macrophages cultured on ALMA 6% displayed significantly higher calprotectin/MR ratio, greater spreading, and increased TNF-α release. These effects can therefore be attributed primarily to stiffness, as topographical differences were negligible. Conversely, while ALMA 2% and 4% hydrogels differed significantly in both roughness and mesh sizes, their storage moduli (G') were not significantly different, and macrophage responses – including calprotectin/MR ratio, eccentricity, cell spreading, and TNF-α, IL-6, and CCL18 release – remained largely similar. Taken together, these findings suggest that nanoscale variations in roughness and mesh size exert little influence on macrophage behaviour in this system, whereas stiffness consistently acts as the key mechanical determinant of macrophage phenotype.

Conclusions

In this study, we show that the stiffness of ALMA hydrogels significantly influences the behaviour of human primary macrophages. Specifically, stiffer hydrogels (~4.5 kPa) promoted a pro-inflammatory phenotype. This was evidenced by the elongated morphology observed on the stiffest hydrogel (ALMA 6%) and a higher calprotectin-to-mannose receptor ratio, indicating a stiffness-dependent, mechano-sensitive shift in macrophage behaviour. These findings were further supported by cytokine profiling, which showed an elevated secretion of TNF-α and IL-6 on stiffer hydrogels compared to softer substrates (~258 Pa). Importantly, this pro-inflammatory response was observed even within the range of soft tissue-relevant stiffness, highlighting the sensitivity of macrophages to subtle mechanical variations. Future studies should explore additional material properties such as viscoelasticity, surface chemistry, and protein adsorption to further elucidate the

complex interactions between biomaterial mechanics and macrophage polarisation. A deeper understanding of how biomechanical properties interface with surface chemistry and protein presentation will guide the rational design of immunomodulatory biomaterials.

Author contributions

Conceptualisation: C. C., J. Y., A. M. G. Data collection: C. C. Writing and reviewing of manuscript: C. C., J. Y., A. M. G. All authors approved the final version of the manuscript.

Conflicts of interest

The authors declare no conflict of interest.

Data availability

Data for this article are available at Research Data Repository (University of Nottingham) at https://rdmc.nottingham.ac.uk/handle/internal/12086.

Supplementary information (SI), including amplitude sweeps (Fig. S1) and roughness (Fig. S2) of ALMA 2%, 4% and 6%, and endotoxin quantification (Fig. S3), is available at https://doi.org/10.1039/d5bm01187f.

Acknowledgements

Funding is acknowledged from the Engineering and Physical Sciences Research Council (EPSRC) & Science Foundation Ireland (SFI) Centre for Doctor Training (CDT) in Transformative Pharmaceutical Technologies (EP/S023054/1), in collaboration with the University of Nottingham. This work was also supported by EPSRC under grant EP/L022494/1. Technical support is acknowledged from: University of Nottingham, Biodiscovery Institute (BDI), Division of Regenerative Medicine and Cellular Therapies (RMCT); University of Nottingham, School of Pharmacy, Boots Science Building; University of Nottingham, School of Life Sciences, Immuno-Bioengineering group; University of Nottingham, Nanoscale & Microscale Research Centre (nmRC).

We would like to acknowledge Dr Hannah Costantin for performing XPS, Ms Nicola J. Weston for performing ESEM, and Dr Long Jiang for performing optical profilometry.

References

1 N. Söhling, M. Ondreka, K. Kontradowitz, T. Reichel, I. Marzi and D. Henrich, Early Immune Response in Foreign Body Reaction Is Implant/Material Specific, *Materials*, 2022, **15**(6), 2195, DOI: 10.3390/ma15062195.

2 N. Noskovicova, B. Hinz and P. Pakshir, Implant Fibrosis and the Underappreciated Role of Myofibroblasts in the Foreign Body Reaction, *Cells*, 2021, **10**(7), 1794, DOI: 10.3390/cells10071794.

3 W.-J. Hu, J. W. Eaton, T. P. Ugarova and L. Tang, Molecular basis of biomaterial-mediated foreign body reactions, *Blood*, 2001, **98**(4), 1231–1238, DOI: 10.1182/blood.V98.4.1231.

4 A. Carnicer-Lombarte, S. T. Chen, G. G. Malliaras and D. G. Barone, Foreign Body Reaction to Implanted Biomaterials and Its Impact in Nerve Neuroprosthetics, *Front. Bioeng. Biotechnol.*, 2021, **9**, 622524–622524, DOI: 10.3389/fbioe.2021.622524.

5 J. C. Doloff, O. Veiseh, A. J. Vegas, H. H. Tam, S. Farah, M. Ma, J. Li, A. Bader, A. Chiu, A. Sadraei, *et al.*, Colony stimulating factor-1 receptor is a central component of the foreign body response to biomaterial implants in rodents and non-human primates, *Nat. Mater.*, 2017, **16**(6), 671–680, DOI: 10.1038/NMAT4866.

6 C. Z. Han, I. J. Juncadella, J. M. Kinchen, M. W. Buckley, A. L. Klibanov, K. Dryden, S. Onengut-Gumuscu, U. Erdbrügger, S. D. Turner and Y. M. Shim, Macrophages redirect phagocytosis by non-professional phagocytes and influence inflammation, *Nature*, 2016, **539**(7630), 570–574.

7 L. C. Davies, S. J. Jenkins, J. E. Allen and P. R. Taylor, Tissue-resident macrophages, *Nat. Immunol.*, 2013, **14**(10), 986–995.

8 K. Karlinsey, L. Qu, A. J. Matz and B. Zhou, A novel strategy to dissect multifaceted macrophage function in human diseases, *J. Leukocyte Biol.*, 2022, **112**(6), 1535–1542, DOI: 10.1002/JLB.6MR0522-685R, acccessed 7/8/2025.

9 M. Nahrendorf and F. K. Swirski, Abandoning M1/M2 for a Network Model of Macrophage Function, *Circ. Res.*, 2016, **119**(3), 414–417, DOI: 10.1161/circresaha.116.309194, from NLM.

10 J. O. Abaricia, N. Farzad, T. J. Heath, J. Simmons, L. Morandini and R. Olivares-Navarrete, Control of innate immune response by biomaterial surface topography, energy, and stiffness, *Acta Biomater.*, 2021, **133**, 58–73, DOI: 10.1016/j.actbio.2021.04.021.

11 F. Y. McWhorter, C. T. Davis and W. F. Liu, Physical and mechanical regulation of macrophage phenotype and function, *Cell. Mol. Life Sci.*, 2015, **72**, 1303–1316.

12 N. R. Patel, M. Bole, C. Chen, C. C. Hardin, A. T. Kho, J. Mih, L. Deng, J. Butler, D. Tschumperlin and J. J. Fredberg, Cell elasticity determines macrophage function, *PLoS One*, 2012, **7**(9), e41024.

13 A. K. Blakney, M. D. Swartzlander and S. J. Bryant, The effects of substrate stiffness on the in vitro activation of macrophages and in vivo host response to poly(ethylene glycol)-based hydrogels, *J. Biomed. Mater. Res., Part A*, 2012, **100**(6), 1375–1386, DOI: 10.1002/jbm.a.34104.

14 R. Sridharan, B. Cavanagh, A. R. Cameron, D. J. Kelly and F. J. O'Brien, Material stiffness influences the polarization state, function and migration mode of macrophages, *Acta Biomater.*, 2019, **89**, 47–59, DOI: 10.1016/j.actbio.2019.02.048.

15 Z. Zhuang, Y. Zhang, S. Sun, Q. Li, K. Chen, C. An, L. Wang, J. J. J. P. van den Beucken and H. Wang, Control of Matrix Stiffness Using Methacrylate–Gelatin Hydrogels for a Macrophage-Mediated Inflammatory Response, *ACS Biomater. Sci. Eng.*, 2020, **6**(5), 3091–3102, DOI: 10.1021/acsbiomaterials.0c00295.
16 M. L. Previtera and A. Sengupta, Substrate stiffness regulates proinflammatory mediator production through TLR4 activity in macrophages, *PLoS One*, 2015, **10**(12), e0145813.
17 M. Chen, Y. Zhang, P. Zhou, X. Liu, H. Zhao, X. Zhou, Q. Gu, B. Li, X. Zhu and Q. Shi, Substrate stiffness modulates bone marrow-derived macrophage polarization through NF-κB signaling pathway, *Bioact. Mater.*, 2020, **5**(4), 880–890, DOI: 10.1016/j.bioactmat.2020.05.004.
18 Y. Ni, H. Qi, F. Zhang, S. Jiang, Q. Tang, W. Cai, W. Mo, R. J. Miron and Y. Zhang, Macrophages modulate stiffness-related foreign body responses through plasma membrane deformation, *Proc. Natl. Acad. Sci. U. S. A.*, 2023, **120**(3), e2213837120–e2213837120, DOI: 10.1073/pnas.2213837120.
19 S. Camarero-Espinosa, M. Carlos-Oliveira, H. Liu, J. F. Mano, N. Bouvy and L. Moroni, 3D Printed Dual–Porosity Scaffolds: The Combined Effect of Stiffness and Porosity in the Modulation of Macrophage Polarization, *Adv. Healthcare Mater.*, 2022, **11**(1), e2101415, DOI: 10.1002/adhm.202101415.
20 X. Xing, Y. Wang, X. Zhang, X. Gao, M. Li, S. Wu, Y. Zhao, J. Chen, D. Gao and R. Chen, Matrix stiffness–mediated effects on macrophages polarization and their LOXL2 expression, *FEBS J.*, 2021, **288**(11), 3465–3477.
21 E. Gruber, C. Heyward, J. Cameron and C. Leifer, Toll-like receptor signaling in macrophages is regulated by extracellular substrate stiffness and Rho-associated coiled-coil kinase (ROCK1/2), *Int. Immunol.*, 2018, **30**(6), 267–278.
22 P. V. Taufalele, W. Wang, A. J. Simmons, A. N. Southard-Smith, B. Chen, J. D. Greenlee, M. R. King, K. S. Lau, D. C. Hassane and F. Bordeleau, Matrix stiffness enhances cancer-macrophage interactions and M2-like macrophage accumulation in the breast tumor microenvironment, *Acta Biomater.*, 2023, **163**, 365–377.
23 C. Guenther, Stiffness regulates dendritic cell and macrophage subtype development and increased stiffness induces a tumor–associated macrophage phenotype in cancer co–cultures, *Front. Immunol.*, 2024, **15**, 1434030.
24 R. A. Scott, K. L. Kiick and R. E. Akins, Substrate stiffness directs the phenotype and polarization state of cord blood derived macrophages, *Acta Biomater.*, 2021, **122**, 220–235, DOI: 10.1016/j.actbio.2020.12.040.
25 K. M. Adlerz, H. Aranda-Espinoza and H. N. Hayenga, Substrate elasticity regulates the behavior of human monocyte-derived macrophages, *Eur. Biophys. J.*, 2016, **45**(4), 301–309, DOI: 10.1007/s00249-015-1096-8.
26 F. Krombach, S. Münzing, A.-M. Allmeling, J. T. Gerlach, J. Behr and M. Dörger, Cell size of alveolar macrophages: an interspecies comparison, *Environ. Health Perspect.*, 1997, **105**(suppl 5), 1261–1263.
27 J. H. Patrick, Species differences in the structure and function of the immune system, *Toxicology*, 2003, **188**(1), 49–71, DOI: 10.1016/S0300-483X(03)00043-X.
28 J. Mestas and C. C. Hughes, Of mice and not men: differences between mouse and human immunology, *J. Immunol.*, 2004, **172**(5), 2731–2738.
29 F. O. Martinez, L. Helming, R. Milde, A. Varin, B. N. Melgert, C. Draijer, B. Thomas, M. Fabbri, A. Crawshaw and L. P. Ho, Genetic programs expressed in resting and IL-4 alternatively activated mouse and human macrophages: similarities and differences, *Blood*, 2013, **121**(9), e57–e69.
30 M. Daigneault, J. A. Preston, H. M. Marriott, M. K. Whyte and D. H. Dockrell, The identification of markers of macrophage differentiation in PMA-stimulated THP-1 cells and monocyte-derived macrophages, *PLoS One*, 2010, **5**(1), e8668.
31 K. L. Spiller, E. A. Wrona, S. Romero-Torres, I. Pallotta, P. L. Graney, C. E. Witherel, L. M. Panicker, R. A. Feldman, A. M. Urbanska and L. Santambrogio, Differential gene expression in human, murine, and cell line-derived macrophages upon polarization, *Exp. Cell Res.*, 2016, **347**(1), 1–13.
32 C. F. Guimarães, L. Gasperini, A. P. Marques and R. L. Reis, *Nat. Rev. Mater.*, 2020, **5**(5), 351–370.
33 Y. Shi, K. J. Glaser, S. K. Venkatesh, E. I. Ben-Abraham and R. L. Ehman, Feasibility of using 3D MR elastography to determine pancreatic stiffness in healthy volunteers, *J. Magn. Reson. Imaging*, 2015, **41**(2), 369–375.
34 A. Kolipaka, S. Schroeder, X. Mo, Z. Shah, P. A. Hart and D. L. Conwell, Magnetic resonance elastography of the pancreas: Measurement reproducibility and relationship with age, *Magn. Reson. Imaging*, 2017, **42**, 1–7.
35 H. An, Y. Shi, Q. Guo and Y. Liu, Test–retest reliability of 3D EPI MR elastography of the pancreas, *Clin. Radiol.*, 2016, **71**(10), 1068.
36 R. Pozzi, I. Parzanese, A. Baccarin, M. Giunta, C. B. Conti, P. Cantù, G. Casazza, A. Tenca, R. Rosa and D. Gridavilla, Point shear-wave elastography in chronic pancreatitis: A promising tool for staging disease severity, *Pancreatology*, 2017, **17**(6), 905–910.
37 K. Y. Lee and D. J. Mooney, Alginate: Properties and biomedical applications, *Prog. Polym. Sci.*, 2012, **37**(1), 106–126, DOI: 10.1016/j.progpolymsci.2011.06.003.
38 N. M. Sanchez-Ballester, B. Bataille and I. Soulairol, Sodium alginate and alginic acid as pharmaceutical excipients for tablet formulation: Structure-function relationship, *Carbohydr. Polym.*, 2021, **270**, 118399–118399, DOI: 10.1016/j.carbpol.2021.118399.
39 D. M. Hariyadi and N. Islam, Current Status of Alginate in Drug Delivery, *Adv. Pharmacol. Pharm. Sci.*, 2020, **2020**, 1–16, DOI: 10.1155/2020/8886095.
40 Q. Liu, A. Chiu, L.-H. Wang, D. An, M. Zhong, A. M. Smink, B. J. de Haan, P. de Vos, K. Keane, A. Vegge, *et al.*, Zwitterionically modified alginates mitigate cellular overgrowth for cell encapsulation, *Nat. Commun.*, 2019, **10**(1), 5262–5214, DOI: 10.1038/s41467-019-13238-7.

41 A. J. Vegas, O. Veiseh, J. C. Doloff, M. Ma, H. H. Tam, K. Bratlie, J. Li, A. R. Bader, E. Langan, K. Olejnik, *et al.*, Combinatorial hydrogel library enables identification of materials that mitigate the foreign body response in primates, *Nat. Biotechnol.*, 2016, **34**(3), 345–352, DOI: 10.1038/nbt.3462.

42 S. Fateh, R. A. Alromaihi, A. M. Ghaemmaghami and M. R. Alexander, Unlocking Bio-Instructive Polymers: A Novel Multi-Well Screening Platform Based on Secretome Sampling, *Bio-Protoc*, 2024, **14**(4), e4939.

43 V. Richterová, A. Gjevik, O. Vaculík, J. Vejrosta and M. Pekař, Impact of Collagen on the Rheological and Transport Properties of Agarose Hydrogels, *Gels*, 2025, **11**(6), 396, DOI: 10.3390/gels11060396.

44 M. Vassey, L. Ma, L. Kämmerling, C. Mbadugha, G. F. Trindade, G. P. Figueredo, F. Pappalardo, J. Hutchinson, R. Markus and S. Rajani, Innate immune cell instruction using micron-scale 3D objects of varied architecture and polymer chemistry: The ChemoArchiChip, *Matter*, 2023, **6**(3), 887–906.

45 M. J. Vassey, G. P. Figueredo, D. J. Scurr, A. S. Vasilevich, S. Vermeulen, A. Carlier, J. Luckett, N. R. M. Beijer, P. Williams, D. A. Winkler, *et al.*, Immune Modulation by Design: Using Topography to Control Human Monocyte Attachment and Macrophage Differentiation, *Adv. Sci.*, 2020, **7**(11), 1903392, DOI: 10.1002/advs.201903392.

46 M. S. Rehmann, K. M. Skeens, P. M. Kharkar, E. M. Ford, E. Maverakis, K. H. Lee and A. M. Kloxin, Tuning and Predicting Mesh Size and Protein Release from Step Growth Hydrogels, *Biomacromolecules*, 2017, **18**(10), 3131–3142, DOI: 10.1021/acs.biomac.7b00781, from NLM.

47 A. F. Roca-Arroyo, J. A. Gutierrez-Rivera, L. D. Morton and D. A. Castilla-Casadiego, Hydrogel Network Architecture Design Space: Impact on Mechanical and Viscoelastic Properties, *Gels*, 2025, **11**(8), 588, DOI: 10.3390/gels11080588.

48 M. Hasany, S. Talebian, S. Sadat, N. Ranjbar, M. Mehrali, G. G. Wallace and M. Mehrali, Synthesis, properties, and biomedical applications of alginate methacrylate (ALMA)-based hydrogels: Current advances and challenges, *Appl. Mater. Today*, 2021, **24**, 101150.

49 N. Kalashnikov and C. Moraes, Substrate viscoelasticity affects human macrophage morphology and phagocytosis, *Soft Matter*, 2023, **19**(13), 2438–2445.

50 D. Tao, H. Wang, S. Chang, J. Cheng, N. Da, L. Zhang, J. Yang, W. Wang, F. Xu and B. Li, Matrix Viscoelasticity Orchestrates Osteogenesis via Mechanotransduction Mediated Metabolic Switch in Macrophages, *Adv. Healthcare Mater.*, 2025, **14**(11), 2405097, DOI: 10.1002/adhm.202405097, acccessed 2025/07/21.

51 O. Chaudhuri, J. Cooper-White, P. A. Janmey, D. J. Mooney and V. B. Shenoy, Effects of extracellular matrix viscoelasticity on cellular behaviour, *Nature*, 2020, **584**(7822), 535–546.

52 H. M. Rostam, L. E. Fisher, A. L. Hook, L. Burroughs, J. C. Luckett, G. P. Figueredo, C. Mbadugha, A. C. K. Teo, A. Latif and L. Kämmerling, Immune-instructive polymers control macrophage phenotype and modulate the foreign body response in vivo, *Matter*, 2020, **2**(6), 1564–1581.

53 M. A. Heinrich, L. Heinrich, M. J. K. Ankone, B. Vergauwen and J. Prakash, Endotoxin contamination alters macrophage-cancer cell interaction and therapeutic efficacy in pre-clinical 3D in vitro models, *Biomater. Adv.*, 2023, **144**, 213220, DOI: 10.1016/j.bioadv.2022.213220.

54 R. G. Wells, The role of matrix stiffness in regulating cell behavior, *Hepatology*, 2008, **47**(4), 1394–1400.

55 A. Santos and D. Lagares, Matrix stiffness: the conductor of organ fibrosis, *Curr. Rheumatol. Rep.*, 2018, **20**, 1–13.

56 A. Vedadghavami, F. Minooei, M. H. Mohammadi, S. Khetani, A. R. Kolahchi, S. Mashayekhan and A. Sanati-Nezhad, Manufacturing of hydrogel biomaterials with controlled mechanical properties for tissue engineering applications, *Acta Biomater.*, 2017, **62**, 42–63.

57 M. Bartnikowski, R. M. Wellard, M. Woodruff and T. Klein, Tailoring hydrogel viscoelasticity with physical and chemical crosslinking, *Polymers*, 2015, **7**(12), 2650–2669.

58 A. Elosegui-Artola, A. Gupta, A. J. Najibi, B. R. Seo, R. Garry, C. M. Tringides, I. de Lázaro, M. Darnell, W. Gu, Q. Zhou, *et al.*, Matrix viscoelasticity controls spatiotemporal tissue organization, *Nat. Mater.*, 2023, **22**(1), 117–127, DOI: 10.1038/s41563-022-01400-4.

59 O. Chaudhuri, L. Gu, M. Darnell, D. Klumpers, S. A. Bencherif, J. C. Weaver, N. Huebsch and D. J. Mooney, Substrate stress relaxation regulates cell spreading, *Nat. Commun.*, 2015, **6**(1), 6365, DOI: 10.1038/ncomms7365.

60 E. Hui, K. I. Gimeno, G. Guan and S. R. Caliari, Spatiotemporal Control of Viscoelasticity in Phototunable Hyaluronic Acid Hydrogels, *Biomacromolecules*, 2019, **20**(11), 4126–4134, DOI: 10.1021/acs.biomac.9b00965.

61 D. Indana, P. Agarwal, N. Bhutani and O. Chaudhuri, Viscoelasticity and adhesion signaling in biomaterials control human pluripotent stem cell morphogenesis in 3D culture, *Adv. Mater.*, 2021, **33**(43), 2101966.

62 R.-Q. Chen, P.-J. Liu, S. Li, H.-P. He, D.-M. Li, G.-X. Yuan, X.-Y. Du, J.-Y. Su, Z.-H. Deng and J. Xu, Healing of tendon-related diseases: insights from macrophage regulation, *Mil. Med. Res.*, 2025, **12**(1), 45, DOI: 10.1186/s40779-025-00635-x.

63 W. Bu, Y. Wu, A. M. Ghaemmaghami, H. Sun and A. Mata, Rational design of hydrogels for immunomodulation, *Regener. Biomater.*, 2022, **9**, rbac009, DOI: 10.1093/rb/rbac009.

64 T. C. Yadav and A. Bachhuka, Tuning foreign body response with tailor-engineered nanoscale surface modifications: fundamentals to clinical applications, *J. Mater. Chem. B*, 2023, **11**(33), 7834–7854.

65 D. W. Dumbauld, T. T. Lee, A. Singh, J. Scrimgeour, C. A. Gersbach, E. A. Zamir, J. Fu, C. S. Chen, J. E. Curtis and S. W. Craig, How vinculin regulates force transmission, *Proc. Natl. Acad. Sci. U. S. A.*, 2013, **110**(24), 9788–9793.

66 H. M. Rostam, S. Singh, F. Salazar, P. Magennis, A. Hook, T. Singh, N. E. Vrana, M. R. Alexander and

A. M. Ghaemmaghami, The impact of surface chemistry modification on macrophage polarisation, *Immunobiology*, 2016, **221**(11), 1237–1246.

67 M. Shen and T. A. Horbett, The effects of surface chemistry and adsorbed proteins on monocyte/macrophage adhesion to chemically modified polystyrene surfaces, *J. Biomed. Mater. Res.*, 2001, **57**(3), 336–345.

68 E. Buck, S. Lee, L. S. Stone and M. Cerruti, Protein adsorption on surfaces functionalized with COOH groups promotes anti-inflammatory macrophage responses, *ACS Appl. Mater. Interfaces*, 2021, **13**(6), 7021–7036.

69 T. T. Lee, J. R. García, J. I. Paez, A. Singh, E. A. Phelps, S. Weis, Z. Shafiq, A. Shekaran, A. Del Campo and A. J. García, Light-triggered in vivo activation of adhesive peptides regulates cell adhesion, inflammation and vascularization of biomaterials, *Nat. Mater.*, 2015, **14**(3), 352–360.

70 P. R. L. Dabare, A. Bachhuka, J. Y. Quek, L. F. Marsal, J. Hayball and K. Vasilev, Nano–Roughness–Mediated Macrophage Polarization for Desired Host Immune Response, *Small Sci.*, 2023, **3**(10), 2300080.

71 N. Ferraz, J. Hong, M. Santin and M. Karlsson Ott, Nanoporosity of Alumina Surfaces Induces Different Patterns of Activation in Adhering Monocytes/Macrophages, *Int. J. Biomater.*, 2010, **2010**(1), 402715, DOI: 10.1155/2011/402715, acccessed 2025/09/15.